A Study of Gas-Centered Swirl Coaxial Injectors Using X-ray Radiography

S.A. Schumaker[1*], A.L. Kastengren[2], M.D.A. Lightfoot[1], S.A. Danczyk[1] and C.F. Powell[2]
[1]Air Force Research Laboratory, Edwards AFB, CA, USA
[2]Argonne National Laboratory, Argonne, IL, USA

Abstract

Gas-centered swirl coaxial injectors, a specific type of airblast atomizer, are of interest in rocket propulsion applications. These applications require good mixing of the liquid and gas to ensure complete combustion within the engine. While strides are being made on the computational front, predictions of the mass distributions achieved with this type of injector remain too costly or too inaccurate for engineering design. There has been, therefore, a reliance on experimental results. Unfortunately, the mass flow rates and the strong gas phase momentum typically encountered in rocket engines create sprays with high optical densities and render the vast majority of optical and laser techniques ineffective in the near-injector region. Data has been obtainable through mechanical patternation, but the technique has limitations. Time-gated ballistic imaging has also shown promise in rocket injectors but produces quantatitve data only on the size and shape of spray structures. An x-ray radiographic technique with a high-brillance x-ray source (Advanced Photon Source) has been applied to these high-optical-density sprays. To achieve this testing a new, mobile flow facility was constructed; this facility simulates the rocket flows using water and nitrogen instead of fuel and oxidizer. The x-ray radiography technique has been able to measure equilvent path length in gas-centered swirl coaxial injectors at a range of typical operating conditions. These results and their implications for gas-centered swirl coaxial injector performance in liquid rocket engines are discussed.

Introduction

For decades the rocket community has struggled to make measurements in the near-injector region of rocket-relevant sprays, especially with injectors that rely on a strong gas phase flow to drive primary atomization. Visible-light techniques such as PDPA, shadowgraphy, laser absorption and laser diffraction all suffer from multiple scattering effects [1]. Mechanical pattenization and flow splitting for visible-light techniques are possible [2] but intrusive and can greatly alter the flow field in the near-injector region. Ballistic imaging overcomes both of these limitations, but is limited to images where only the size and shape of spray structures can be obtained and not all mass is captured [3]. To further a physics-based understanding of shear-driven rocket injectors a quantitative nonintrusive diagnostic technique that does not suffer from multiple scattering effects is required.

X-ray radiography is an attractive alternative to visible-light and intrusive techniques since in the x-ray part of the spectrum the dominant interaction of photons with droplets is absorption rather than elastic scattering. Since absorption is the dominant mechanism, Beer's Law can be used to solve for the liquid-phase thickness along the integrated path length. Recently, x-ray radiography has been successfully applied in the study of diesel injectors, aerated liquid jets, solid-cone sprays and impinging-jet sprays [4-7]. While x-ray radiography can be performed using either a synchrotron source or a tube source, a synchrotron source has a number of well-documented advantages over a tube source such as enough flux to allow filtering to produce a monochromatic beam [8]. The one large disadvantage of a synchrotron source is that the experiment must be brought to a synchrotron facility. Such facilities typically lack the infrastructure necessary to deliver high-pressure liquid and gas at sufficient flow rates for rocket-injector testing. To overcome this lack of infrastructure the Mobile Flow Laboratory (MFL) was recently constructed; it is capable of delivering water and gaseous nitrogen at flow rates on the order of 450 g/s and pressures in excess of 130 atm. The facility fits into the 7-BM beamline test hutch of the Advanced Photon Source (APS) located at Argonne National Laboratory (ANL).

X-ray radiography measurements were made in the near-injector region of a number of Gas-Centered Swirl Coaxial (GCSC) injectors. These injectors are a type of prefilming airblast atomizer that has seen an increase in interest over the last decade due to their high performance at flow conditions typical of OX-rich staged combustion cycles. The authors have previously developed physics-based scaling laws for these injectors and experimentally investigated the effect of momentum flux ratio and geometric variations on the film length and spray structures [9, 10]. The results presented in this paper are the first quantitative internal spray measurements ob-

* Corresponding author: Stephen.Schumaker@edwards.af.mil

tained in the near-injector region for this injector type. X-ray radiography measurements are used to investigate the effect of liquid swirl and momentum flux ratio on the spray structure.

Experimental Methods

Gas-centered swirl-coaxial injectors are a type of airblast atomizer which utilizes an axial, fast-moving gas stream to strip droplets from a swirling, wall bounded film. Unswirled gas enters down the centerline of the injector while the film is created by introducing liquid through holes tangentially drilled into the injector cup. A sketch of this injector is shown in Fig. 1. In past studies a number of different injector configurations have been examined [9,10]. In the current study the same injector cup geometry with three different liquid-inlet configurations was used. Different liquid-inlet configurations allow for varying degrees of swirl. The baseline injector body has four tangential inlet holes of diameter 1.60 mm and an axial-to-total velocity ratio (R_A) of 30%. This inlet configuration is designated by 4H-Φ where Φ is the momentum flux ratio of the test condition. The other two injector bodies use an eight-hole configuration. The first eight-hole configuration has the same inlet diameter as the four-hole configuration—in other words double the liquid-inlet flow area—producing an R_A value of 41%. The double-area configuration is designated by 8HDA-Φ. The second eight-hole configuration has approximately the same inlet area as the baseline injector but twice the number of holes (hole diameters of 0.989 mm) producing a R_A of 26%. The same-area case is designated by 8HSA-Φ. Swirl quantities are given in terms of the axial-to-total velocity ratios because the swirl number, typically designated by tangential over total velocity, is close to 1 and difficult to distinguish between cases. The gas post is 180 mm in length with a fixed radius of 6.35 mm resulting in a gas inlet L/D ratio of ~14.

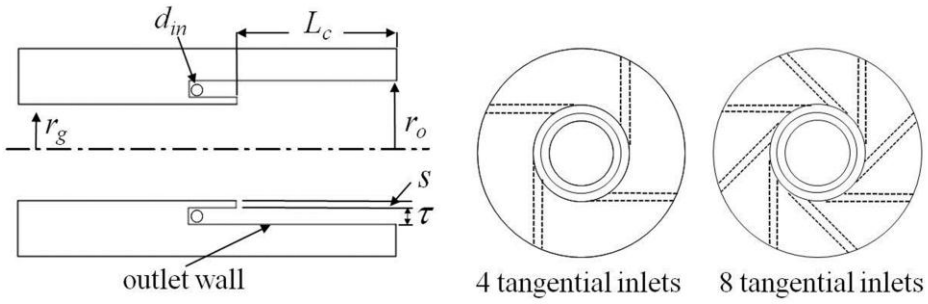

Figure 1. Schematic of a gas-centered swirl-coaxial injector where r_g represents the gas post radius (6.35 mm), L_c the injector cup length (33.0 mm), r_o the outlet radius (9.53 mm), S the step height (1.52 mm), τ the initial film thickness (1.65 mm), and d_{in} the liquid inlet diameter. Four- and eight-hole liquid inlet geometries are shown.

Surrogate propellants (water and gaseous nitrogen) were delivered to the injector using a newly constructed facility dubbed the Mobile Flow Laboratory (MFL). The MFL was designed to allow aerospace-propulsion injector testing at remote diagnostic facilities such as APS that do not have the infrastructure to provide relevant flow conditions. The MFL is a self-contained system with its own data acquisition and control systems allowing it to be run remotely. Liquid nitrogen, electrical power and an exhaust system are all that is required of the host facility. Gaseous nitrogen is produced from the liquid supply and is stored in two, 57-liter gas bottles. The gaseous nitrogen is also used to pressurize a 57-liter water tank. Gas and liquid flow rates are controlled using electronic pressure regulators with calibrated critical flow orifices. The system has an uncertainly of 4% in the gas flow rate and 1% in the liquid flow rate [11]. Gaseous flow rates were between 33-46 g/s and water rates between 22-49 g/s for the current study (well below maximum capabilities).

X-ray radiography measurements were performed at the 7-BM beamline at the Advanced Photon Source. The x-ray source for the beamline is a synchrotron bending magnet. This source produces polychromatic, nearly collimated radiation. A double-multilayer monochromator is used to produce a monochromatic ($\Delta E/E$=1.4%) x-ray beam. Details regarding the beamline setup are given in Ref. [12]. For the current experiment a beam photon energy of 10 keV was used. Using a pair of Kirkpatrick-Baez focusing mirrors housed in the experimental enclosure the beam was focused to 5 μm vertical x 7 μm horizontal (full width at half maximum) at a flux of 1.6×10^{10} photons per second before the experimental apparatus. A silicon PIN diode was used as the detector. The photocurrent from this PIN diode was amplified and time averaged over a 4 second integration time. One-dimensional scans were made across the spray, perpendicular to the injector with a 0.5 mm step size; each scan consisted of 97 points. For every flow condition scans were performed 3, 5, 7.5, 10 and 20 mm downstream of the injector face at a minimum of three different rotation angles (nominally 0^o, 60^o, and 300^o). However, a select number of cases had additional angles, including 180^o, that allowed the effect of gravity to be explored for these horizontally flowing sprays.

The recorded signal level was converted to the Equivalent Path Length (EPL) of water using Beer's law

$$EPL = \frac{-\ln(I/I_0)}{\beta\rho}\,, \tag{1}$$

where I is the intensity of the transmitted light, I_0 is the intensity of incident light, β is the mass attenuation coefficient, and ρ is the density of the absorbing fluid. Normalization by I_o was performed in two steps. First, each point in the scan was normalized by a corresponding beam intensity measured from an intensity monitor based on fluorescence from a thin titanium foil placed inline with the beam upstream of the spray. The I_o measurement accounts for changes in beam intensity during a scan. A complete 97 point scan took approximately 8 minutes. The second normalization baselines the intensity to the zero absorption case and uses the average signal level from the 5 points in the scan with the highest transmissions. These were points that are outside of the spray. The mass attenuation coefficient can be calculated using the NIST photon cross section database [13]; for pure water and a beam energy of 10 keV is 5.33 cm^2/g. The EPL is the pathlength-integral of the amount of water in the beam. Interpretation of the EPL is discussed further in the Results and Discussion section. It should be noted that the use of monochromatic x-rays greatly simplifies the conversion of x-ray transmission to EPL; this is a significant advantage of synchrotron sources over laboratory x-ray sources.

In addition to x-ray radiography measurements, high-speed shadowgraphy images were taken of all flow conditions. A 600W, DC light source in combination with a Vision Research Phantom V7.3 camera was used to obtain images at 6006 fps. An in-house Matlab routine employing image segregation techniques was used to measure spray widths [14]. Note that for radiography measurements the spray was horizontally oriented and flowed into an exhaust duct; for shadowgraphy images the spray was vertically oriented and flowed into a large pit.

Scaling & Test Matrix

Previous studies have shown that GCSC injectors in liquid rocket engines operate in a high Weber and Reynolds number regime. Here aerodynamic forces dominate and, therefore, the main atomization mechanism is stripping/tearing resulting from gas-phase vortices. This atomization mechanism results in the momentum flux ratio being the dominant scaling parameter [15]. The momentum flux ratio is defined as $\Phi = \left(\rho_g/\rho_l\right)/\left(v_g/v_l\right)^2$, where v is the velocity and subscripts g and l distinguish the gas and liquid phase, respectively. While the basic equation for Φ is simple, care must be taken in defining the relevant densities and velocities. Earlier work showed the best collapse of measured film lengths with Φ when the gas density and velocity at the gas post lip is calculated using one-dimensional compressible gas dynamics along with measured static pressure and total temperature. On the liquid side the total liquid velocity assuming conservation of momentum between the tangential inlet hole outlets and the gas post lip produces the best fit [9].

While not as strong as the aerodynamic forces, the centripetal force is expected to play some role in the atomization process. The centripetal force acts opposite of the aerodynamic forces to stabilize the film by decreasing the size and growth rate of any disturbances caused by the aerodynamic forces on the film surface. In addition, the entrainment of gas into the liquid film is hindered by the buoyancy-type force created from the centripetal acceleration. Mass flow rates and values of the nondimensional parameters are given in Table 1. Full definitions of the nondimensional parameters can be found in Ref. [9].

Table 1. Test conditions with mass flow rates and relevant nondimensional parameters.

Condition	$\dot{m}_g$ (g/s)	$\dot{m}_l$ (g/s)	Φ_{total}	R_A	Re_g	Re_l	We	Fr_c
4H-60	46	37	58	0.299	380,000	2,100	42	0.158
4H-90	46	30	86	0.299	380,000	1,800	29	0.158
4H-120	46	26	117	0.299	380,000	1,500	21	0.158
4H-145	46	23	141	0.299	380,000	1,400	17	0.158
8HSA-60	46	32	58	0.261	380,000	2,200	42	0.162
8HSA-90	46	26	89	0.261	380,000	1,800	28	0.162
8HSA-110	54	26	107	0.261	440,000	1,800	28	0.162
8HSA-120	46	22	120	0.261	380,000	1,600	20	0.162
8HDA-60	46	49	60	0.406	380,000	2,100	41	0.145
8HDA-90	46	40	91	0.406	380,000	1,700	27	0.145
8HDA-120	46	35	118	0.406	370,000	1,600	21	0.145
8HDA-130	33	26	128	0.406	260,000	1,100	12	0.145
8HDA-145	46	31	148	0.406	380,000	1,364	17	0.145

Results and Discussion

Care must be taken when interpreting x-ray radiography measurements. X-ray radiography measures the path-integrated average liquid density which can be given as an Equivalent Path Length (EPL) of the liquid. Interpretation can be complex since in additional to being path integrated these parameters are a function of both the local mass flux and the velocity field. This is only true for a spray, not for say, in a column of water. Profiles of EPL are shown in Fig. 2a for test condition 8HSA-120 at a scan angle of 60° and five downstream locations. The EPL profiles in Fig. 2a show peaks on the edge of the spray and a trough in the middle of the spray. The two-dimensional near-injector EPL field can be obtained by interpolating between the profiles (Fig. 2b). The bimodal shape of the distributions indicates, at an instant in time, a higher density on the spray periphery and a lower density in the core. Since the peaks near the edge of the spray are in a region of small spray cord length, the peaks indicate an area of high mass flux and/or slow velocity. The valley centred on r=0 mm, which is the largest path length, indicates an area of lower mass flux and/or faster velocity. For the GCSC injectors used in this work, nonuniformities in both the velocity and mass flux fields are likely responsible for these profiles but the high velocity along the spray's centerline is by far the largest driver.

For the case shown in Fig. 2a, the bulk velocity at the gas-post exit is approximately 300 m/s. With the atomization of the liquid film occurring at the injector cup wall, a boundary-layer-like velocity deficit is created at the edge of the spray where droplet velocities are on the order of tens of meters per second. The axial distribution of the droplet formation is also likely playing a role. Droplets that have migrated to the center of the spray were likely formed early in the atomization process and therefore have had more time to accelerate and undergo secondary breakup. To fully deconvolve the effects of mass distribution and the droplet velocity field on the EPL an additional measurement of the mass flux or the velocity field is required. This could be accomplished using either a mechanical patternator to obtain mass flux distribution (however this is likely impractical in the near-injector region) or time-resolved x-ray radiography to obtain droplet size and velocity distributions [16].

Figure 2a also shows that the droplets across the entire spray are undergoing acceleration in the near-injector region. Between 3 and 5 mm downstream the spray width is unchanged yet a decrease in the EPL is seen across the entire profile, since the mass flux is unchanged the velocity must be increasing. The acceleration in the near field can be quantified by looking at the mass-weighted velocity at the various downstream locations. The mass-

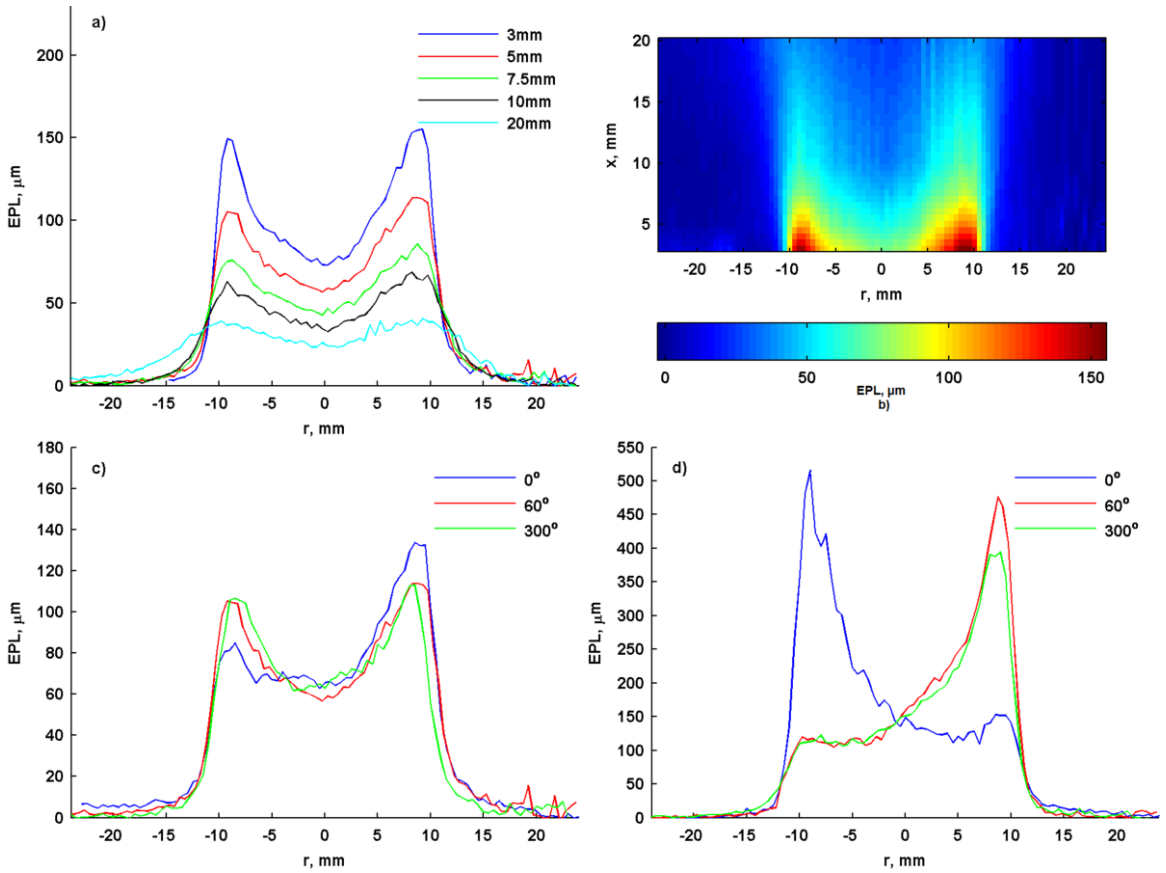

Figure 2. Radial profiles of EPL at a) various downstream locations, b) interpolated color map, and c) scan angles 5 mm downstream for test condition 8HSA-120. d) Radial profiles of EPL at various scan angles 5 mm downstream for test condition 4H-60.

weighted velocity (V_{ma}) is obtained by dividing the liquid mass flow rate with the integral of the integrated average liquid density profile [17]. This double integral first integrates along the beam pathlength and then across the spray so all liquid mass in the 2D cross-section perpendicular to the injector axis is counted. In other words, the EPL is integrated over/across the measurement path perpendicular to the spray axis. Figure 3 shows V_{ma} for the three injector geometries operating at Φ=120. Mass-weighted velocities 3 mm downstream start between 6 and 8 m/s and accelerate to between 17 and 22 m/s by 20 mm downstream. These velocities near the injector exit indicate that, on average, the droplet field has undergone acceleration on the order of 1,000 m/s^2 since the liquid exits the sheltered area at ~0.5 m/s axial velocity. Between 3 and 10 mm, acceleration downstream is on the order of 10,000 m/s^2. By 20 mm, acceleration appears to be decreasing, but a lack of data downstream makes it impossible to know where V_{ma} will asymptote. Smaller velocities for 8HDA-120 are due to large, slow moving droplets on the spray periphery which have been observed in shadowgraphy images (Fig. 7).

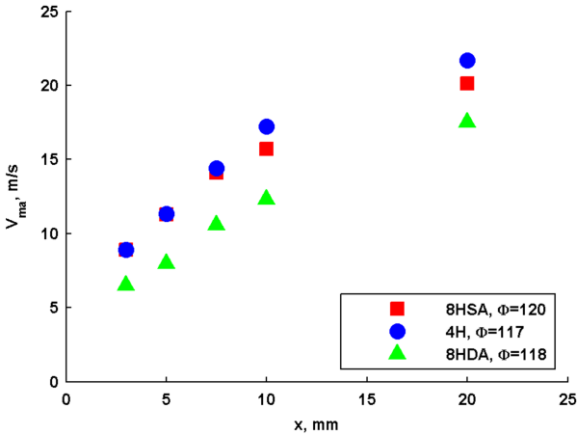

Figure 3. Mass-weighted velocity versus downstream distance for test conditions 4H-120, 8HSA-120, and 8HDA-120.

When looking at the data set as a whole it is clear that all conditions have some level of asymmetry and that a single scan angle is insufficient to fully characterize the spray. Figure 2c shows three scan angles for the 8HSA-120 test condition at 5 mm downstream. This condition, with its high Φ and swirl level, is one of the more uniform conditions in the data set and yet differences in the peak heights are clearly visible along with differences in the spray width. The difference in spray width indicates an ovoid cross-sectional shape. The asymmetry can be substantial as shown in Fig. 2d which shows three scan angles for test condition 4H-60. In this case the film has not fully atomized in the injector cup and ligament-like structures are exiting on only on a portion of the spray periphery. This type of spray nonuniformity has been documented in previous work using laser sheet imaging of the interface between the liquid gas interface and qualitative spray shadowgraphy [10].

Because of space constraints at the 7-BM beamline, testing was conducted with the spray flowing horizontally. Potential gravity effects were investigated in two cases by taking scans 180° apart. Figure 4 shows 0° and 180° scan angles for 8HSA-90 and 8HSA-110. The 180° scan angle was flipped about r=0 to facilitate comparison. Condition 8HSA-110 (Fig. 4a) shows agreement well within any experimental error. The agreement for test condition 8HSA-90 (Fig. 4b) is not as good with the 180° case having one peak lower and one peak higher than the 0° case. The exact cause of this difference is unknown, but is likely not directly related to gravity effects since the direction of increase in EPL is opposite of the gravity vector. Given these results it is unlikely that gravity has more than a minor effect. To address this issue, future testing should include additional scans taken at multiple angles along with their 180° counterparts as well as repeatability studies.

The momentum flux ratio is the single most important nondimensional parameter for determining the atomiza-

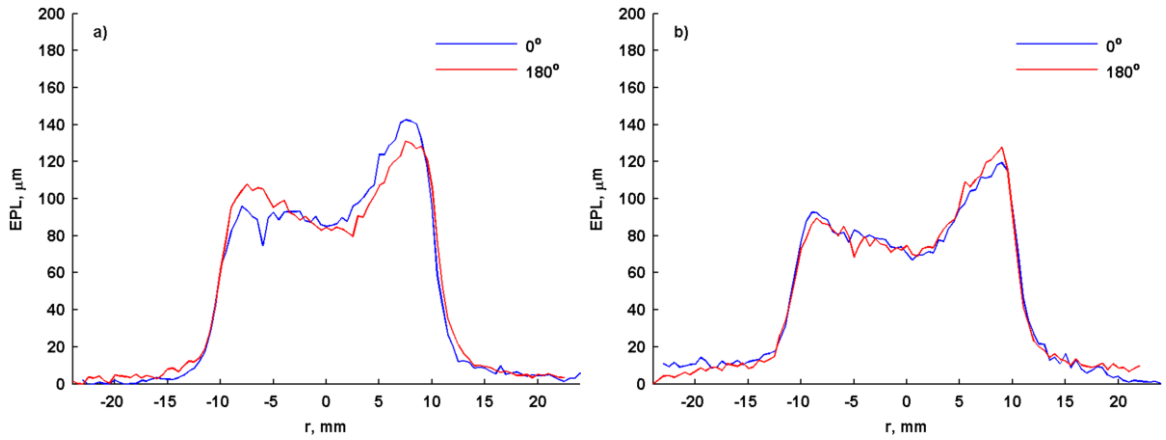

Figure 4. Radial profiles of EPL taken 180° apart at 5 mm downstream for test condition a) 8HSA-90 and b) 8HSA-110. Profiles taken at 180° are flipped around r=0 to better show agreement with 0° scans.

tion efficiency of a GCSC injector [15]. Previous work has shown the film length scales with Φ [9] and shadowgraphy images have shown a decrease in spray quality as Φ decreases [14]. The decrease in spray quality can be quantified using the x-ray radiography measurements. Figure 5 shows EPL profiles for the 4H geometry operating at four different momentum flux ratios; two different scan angles are included. The increase in asymmetry as Φ is decreased is clear for both scan angles. As Φ is increased the profiles become relatively symmetric. Above a certain momentum flux ratio, Φ=117 in the case of Fig. 5, additional improvement becomes minimal. It should also be noted that magnitude differences in the EPL profiles are due in part to different liquid flow rates. For these conditions the gas flow rate is held constant at 46 g/s which results in decreasing liquid flow rates with increasing Φ values. The scaling theory indicates that atomization efficiency should be independent of the liquid flow rate, assuming that the momentum flux ratio is held constant, so it is expected that the symmetry differences in Fig. 5 are driven by Φ and not liquid flow rate. An additional finding from Fig. 5 is that the spray width changes minimally with Φ. The unchanging spray width agrees with shadowgraphy results. The trends based on the 4H geometry are representative of the trends seen across all of the geometries.

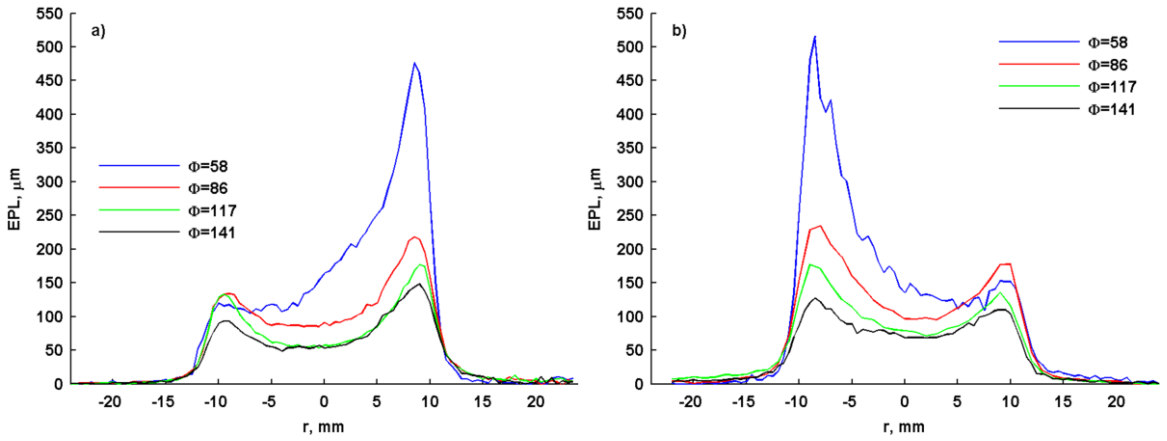

Figure 5. Radial profiles of EPL for test geometry 4H 5 mm downstream operating at varying momentum flux ratios at orientations of a) 60° and b) 0°.

While the spray width does not vary with momentum flux ratio it does vary with swirl level. Figure 6a-b shows the three injector geometries for the same nominal momentum flux ratio (120) at two different scan angles. Across all three angles the spray width decreases with decreasing R_A values (increasing levels of swirl). The axial-to-total velocity ratios for 8HSA, 4H, and 8HDA are 26, 30, and 41%, respectively. As with varying the momentum flux ratio (Fig. 5) the conditions shown in Fig. 6 a-b have the same gas flow rates. The highest swirl case (8HSA) has the lowest liquid flow rate and the lowest swirl case (8HDA) has the highest liquid flow rate. The difference in the total liquid flow rate is clearly seen in the varying heights of the EPL profiles.

To separate the effect of swirl from the liquid flow rate, the same liquid flow rate (26 g/s) was run while the gas flow rate was varied for each swirl level. Conditions with the same liquid flow rate are shown in Fig. 6d. Figure 6d shows the same decrease in width as seen in Fig. 6a-b. While there is some variation in Φ between these conditions, given the previous result that the spray width was unchanged by momentum flux ratio there is little doubt that the changing width is a function of swirl. The decrease in spray width with increasing swirl number is opposite of what would be expected from centripetal force arguments. While the liquid film is atomized prior to exiting the injector cup the droplets may retain some of the film's tangential momentum. Shadowgraphy images (Fig. 7) show that lower-swirl cases with the same momentum flux ratio have larger droplets on the spray periphery. These larger droplets do not get drawn into the center spray and accelerate slowly compared to smaller droplets produced in high swirl cases and are likely causing larger spray widths in the near field.

In an effort to allow closer comparison between the EPL profiles with different liquid flow rates an attempt was made to normalize by the liquid flow rate. Normalizing by the liquid flow rate does bring the profiles closer together, but dissimilarities still exist in the peaks due to different spray asymmetries between the cases (Fig. 6c). Note that differences in profile heights in Fig. 6d are due to differences in the liquid velocity caused by the differing gas flow rates. Interestingly, normalization by the liquid flow rate decreases the difference in spray widths for varying swirl. However, the general trend is still the same.

Changing swirl level also affects spray symmetry; changes can be seen in the two scan angles shown in Fig. 6a-b. In general, as the swirl is increased the spray symmetry improves. For the Φ=120 conditions shown in Fig. 6 the difference in symmetry between 8HSA and 4H is minimal; however, 8HDA, the lowest swirl case, still has substantial asymmetry at this high momentum flux ratio. Note that these conclusions are based on the data set as a whole and not just the plots shown in Fig. 6. This difference in symmetry is directly related to the changes in spray quality seen in shadowgraphy images (Fig. 7).

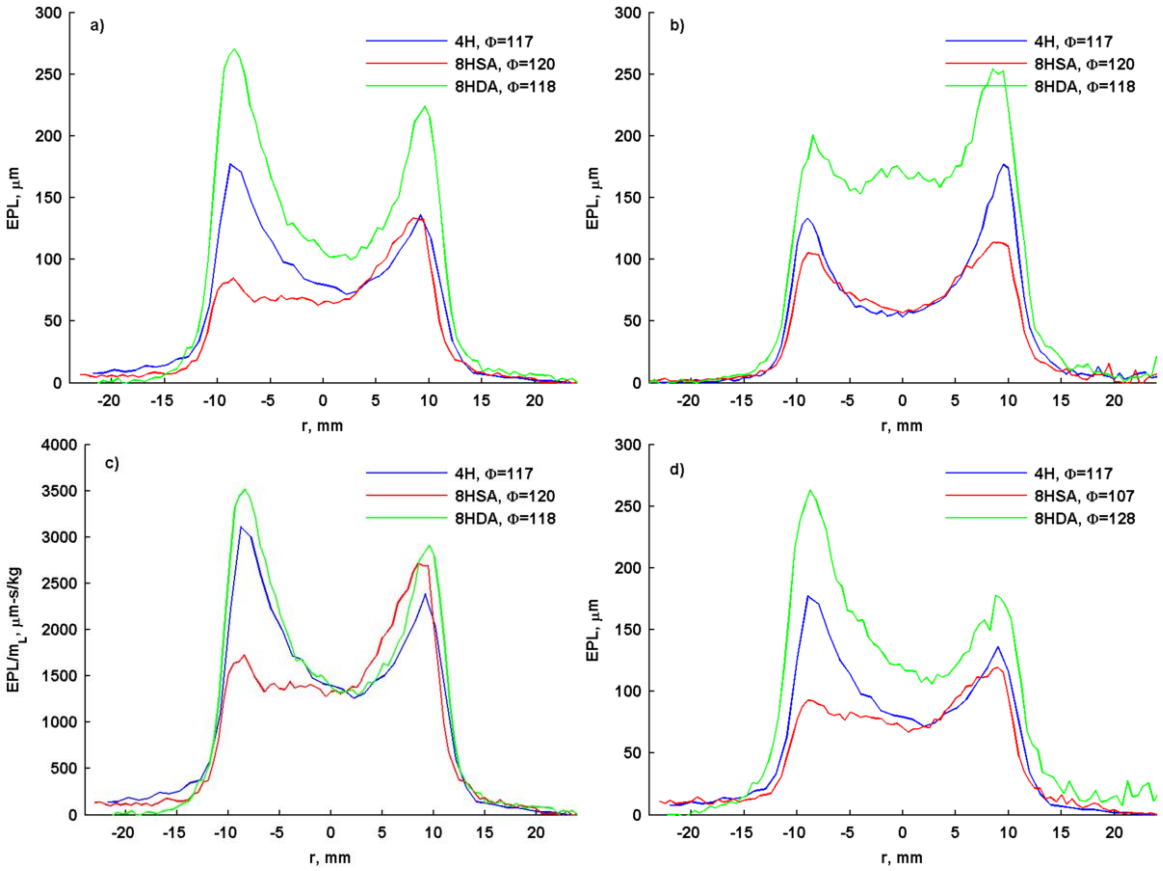

Figure 6. Comparing radial profiles of EPL 5mm downstream for the three injector geometries operating at Φ~100 for a) 0° and b) 60° orientations. c) Radial profile of EPL normalized by the liquid mass flow rate 5mm downstream for the three injector geometries operating at Φ~100 for 0° orientation. d) Radial profiles of EPL for the three injector geometries operating at the same liquid mass flow rate (26 g/s).

R_A=0.299, 4H-120 R_A=0.261, 8HSA-120 R_A=0.406, 8HDA-120

Figure 7. Shadowgraphy spray images. The swirl level has an impact on the quality of the spray as seen by the changes in size and number of structures on the periphery of the spray.

Ballistic imaging indicated that four liquid inlet holes might not be sufficient to create a uniform liquid film exiting the liquid cup [3] and showed remnants of the liquid inlet jets could persist in the spray. Film imaging showed that while the film lengths were comparable between the four and eight hole cases the film profile varied [9]. This current quantitative work, however, shows no measurable difference between the four and eight hole injectors that could not be accounted for by the varying swirl levels.

Summary and Conclusions

X-ray radiography was used to quantitatively examine the near-injector region of GCSC injectors. This work is the first time x-ray radiography has been used in a spray where the atomization is driven by the gas phase. Also, this is the first time quantitative measurements of any kind have been made in the near-injector region of this type of injector. To enable testing, a new mobile test facility was constructed to deliver rocket relevant flow rates and pressures of water and gaseous nitrogen at diagnostic facilities that lack flow infrastructure.

Equivalent path length measurements were presented for three injector geometries and a number of test conditions. Care must be taken when interpreting the EPL in terms of mass flux since the mass flux is a function of both mass and velocity distributions. In the future, time-resolved x-ray measurements may allow the effects of mass and velocity to be separated. In general, EPL profiles showed a peak on each edge of the spray and a valley in the spray center. Higher values indicate areas of increased mass flux and/or decreased velocity and vice versa. EPL profiles also showed asymmetries requiring multiple angles to fully characterize this type of spray. This asymmetry in the spray was found to decrease with increasing momentum flux ratio and increasing level of liquid-film swirl. The width of the spray was found to be unaffected by the momentum flux ratio but did decrease with increasing level of liquid-film swirl. These results agree with qualitative shadowgraphy but allow measures of spray quality such as symmetry to be quantified. Mass-averaged velocities in the near-injector region show that the mass-averaged liquid velocity is much less than the bulk gas-phase velocity and is still undergoing very high acceleration as far downstream as 20 mm. Further work is need to relate EPL to mass and velocity distributions and then to the reacting flow field but it is clear that engines using GCSC injectors must tolerate some level of asymmetry. X-ray radiography has proven itself an important tool that allows quantitative measurements in sprays where other methods fail.

Acknowledgements

A portion of this research was performed at the 7-BM beamline of the Advanced Photon Source, Argonne National Laboratory. Use of the Advanced Photon Source at Argonne National Laboratory was supported by the U. S. Department of Energy, Office of Science, Office of Basic Energy Sciences, under Contract No. DE-AC02-06CH11357. The authors would like to thank Benjamin Halls (Iowa State University), Chad Eberhart (The University of Alabama in Huntsville), and William Miller (Kettering University) for their assistance in set up and data collection during the testing campaign at Argonne National Laboratory.

References

[1] Meyer, T.R., Brear, M., Jin, S.H., and Gord, J.R., *Formation and Diagnostics of Sprays in Combustion: In Handbook of Combustion*, Eds. Lackner, M., Winter, F., and Agarwal, A, Wiley-VCH, 291-322 (2010).
[2] Strakey, P.A., Talley, D.G.,and Hutt, J.J., Journal of Propulsion and Power, 17-2, 402-410 (2001).
[3] Schmidt, J.B. Schaefer, Z.D., Meyer, T.R., Roy, S., Danczyk, S.A., and Gord, J.R., *Applied Optics*, 48 B137-B144 (2009).
[4] Leick, P., Kastengren, A.L., Liu, Z., Wang, J., and Powell, C.F., *11th Triennial International Conference on Liquid Atomization and Spray Systems*, Vail, Colorado, July 2009.
[5] Kastengren, A. L., Powell, C. F., Liu, Z., Moon, S., Gao, J., Zhang, X., and Wang, J., *22nd Annual Conference on Liquid Atomization and Spray Systems*, Cincinnati, Ohio, May 2010.
[6] Lin, K.C., Carter, C., Smith, S., and Kastengren, A., *50th AIAA Aerospace Sciences Meeting*, Nashville, Tennessee, January 2012.
[7] Halls, B. R., Heindel, T.J., Meyer, T.R., and Kastengren, A.L., *50th AIAA Aerospace Sciences Meeting*, Nashville, Tennessee, January 2012.
[8] Heindel, T. J., *Journal of Fluids Engineering*, 133-7, (2011).
[9] Schumaker, S. A., Danczyk, S.A., and Lightfoot M.D.A., *47th AIAA Joint Propulsion Conference*, AIAA-2011-5621, San Diego, California, July 2011.
[10] Schumaker, S. A., Danczyk, S.A., and Lightfoot M.D.A., *48th AIAA Aerospace Sciences Meeting*, AIAA-2010-368, Orlando, Florida, January 2010.
[11] Lightfoot, M.D.A., Danczyk, S.A., Watts, J.M., and Schumaker, S.A., *JANNAF 8th Modeling and Simulation, 6th Liquid Propulsion, and 5th Spacecraft Propulsion Joint Subcommittee Meeting*, Huntsville, Alabama, December 2011, http://handle.dtic.mil/100.2/ADA554591.
[12] Kastengren, A.L., Powell, C. F., Arms, D., Dufresne, E. M., and Wang, J., *22nd Annual Conference on Liquid Atomization and Spray Systems*, Cincinnati, OH, May 2010.
[13] Berger, M.J., Hubbell, J.H., Seltzer, S.M., Chang, J., Coursey J.S., Sukumar, R., Zucker, D.S., and Olsen, K., *XCOM: Photon Cross Sections Database, NIST Standard Reference Database 8 (XGAM)*, http://www.nist.gov/pml/data/xcom/index.cfm.
[14] Lightfoot, M.D.A., Schumaker, S.A., Villasmil, L.A., and Danczyk, S.A., *JANNAF 8th Modeling and Simulation, 6th Liquid Propulsion, and 5th Spacecraft Propulsion Joint Subcommittee Meeting*, Huntsville, Alabama, December 2011, http://handle.dtic.mil/100.2/ADA554873.
[15] Lightfoot, M.D.A., Danczyk, S.A. and Talley, D.G., *19nd Annual Conference on Liquid Atomization and Spray Systems*, Toronto, Canada, May 2006.
[16] Lightfoot, M.D.A., Schumaker, S.A., Danczyk, S.A., and Kastengren, A. L., *24th Annual Conference on Liquid Atomization and Spray Systems*, San Antonio, Texas, May 2012.
[17] Kastengren, A., Powell, C.F., Wang, Y.-J, IM, K.-S., and Wang, J., *Atomization and Sprays*, 19, 1031-1044 (2009).